International Journal of Pharmaceutics 632 (2023) 122527

Contents lists available at ScienceDirect

International Journal of Pharmaceutics

journal homepage: www.elsevier.com/locate/ijpharm

^{61}Cu-Labelled radiodiagnostics of melanoma with NAPamide-targeted radiopharmaceutical

Ibolya Kálmán-Szabó [a,b,1], Szilvia Bunda [c,1], Norbert Lihi [d,*], Zsófia Szaniszló [c], Dezső Szikra [a], Judit Szabó Péliné [a], Anikó Fekete [a], Barbara Gyuricza [a], Dániel Szücs [a], Gábor Papp [c], György Trencsényi [a,b], Ferenc K. Kálmán [c,*]

[a] Division of Nuclear Medicine and Translational Imaging, Department of Medical Imaging, University of Debrecen, Egyetem tér 1., H-4032 Debrecen, Hungary
[b] Gyula Petrányi Doctoral School of Clinical Immunology and Allergology, Faculty of Medicine, University of Debrecen, Nagyerdei St. 98, H-4032 Debrecen, Hungary
[c] Department of Physical Chemistry, University of Debrecen, Egyetem tér 1., H-4032 Debrecen, Hungary
[d] ELKH-DE, Mechanisms of Complex Homogeneous and Heterogeneous Chemical Reactions Research Group, Department of Inorganic and Analytical Chemistry, University of Debrecen, Egyetem tér 1., H-4032 Debrecen, Hungary

ARTICLE INFO

Keywords:
Cu-61
Radiotherapy
Melanoma
Positron emission tomography (PET)
NAPamide

ABSTRACT

Malignant melanoma is a major public health problem with an increasing incidence and mortality in the Caucasian population due to its significant metastatic potential. The early detection of this cancer type by imaging techniques like positron emission tomography acts as an important contributor to the long-term survival. Based on literature data, the radio labelled alpha-MSH analog NAPamide molecule is an appropriate diagnostic tool for the detection of melanoma tumors. Inspired by these facts, a new radiotracer, the [^{61}Cu]Cu-KFTG-NAPamide has been synthesized to exploit the beneficial features of the positron emitter ^{61}Cu and the melanoma specificity of the NAPamide molecule. In this work, we report a new member of the CB-15aneN$_5$ ligand family (KFTG) as the chelator for ^{61}Cu(II) complexation. On the basis of the thorough physico-chemical characterization, the rigid [Cu(KFTG)]$^+$ complex exhibits fast complex formation ($t_{1/2}$ = 155 s at pH 5.0 and 25 °C) and high inertness ($t_{1/2}$ = 2.0 h in 5.0 M HCl at 50 °C) as well as moderate superoxide dismutase activity (IC_{50} = 2.3 μM). Furthermore, the [^{61}Cu]Cu-KFTG-NAPamide possesses outstanding features in the diagnostics of B16-F10 melanoma tumors by PET imaging: (T/M(SUVs) (*in vivo*): appr. 14, %ID/g: 7 ± 1 and T/M (*ex vivo*): 315 ± 24 at 180 min).

1. Introduction

Among skin cancers melanoma malignum is the most aggressive malignancy with high mortality rate and associated with high metastatic potential.(Ahmed et al., 2020) The metastatic lesions in several organs (e.g. brain, liver, lung) largely reduce the chance of patient survival and the five-year survival rate falls between 5 and 19 %.(Sandru et al., 2014) Due to its high metastatic potential, the early diagnosis of small and distant metastases is crucial, thus, high-resolution imaging techniques (e.g. Positron Emission Tomography (PET) or Magnetic Resonance Imaging (MRI)) are frequently used to detect such metastases.(McIvor et al., 2014; Rodriguez Rivera et al., 2014).

In the last decade, several melanoma-specific radiolabeled molecules (e.g. antibodies,(Thompson et al., 2014) α-MSH receptor (alpha-Melanocyte-Stimulating hormone) ligands(Gao et al., 2016) and benzamide derivatives(Kim et al., 2012)) have been developed for PET imaging of melanoma. In the field of nuclear medicine, the melanocortin-1 receptor (MC1-R) – as a G-protein-coupled cell membrane receptor – is one of the most promising targets due to its significant overexpression on the surface of melanoma metastases.(Chung et al., 2012; Rosenkranz et al., 2013) Alpha melanocyte stimulating hormone (α-MSH) analogues, e.g. NAPamide peptide, specifically bind to the MC1-R receptors. For *in vivo* preclinical PET imaging several ^{64}Cu-,Cheng et al., 2007a ^{68}Ga-, ^{44}Sc-,(Nagy et al., 2017) ^{18}F-,(Ren et al., 2009; Cheng et al., 2007b) ^{111}In- and ^{99m}Tc-labelled(Miao et al., 2007) NAPamide analogues are reported as potential melanoma-specific radiopharmaceuticals.

Beyond the widely used ^{64}Cu isotope, the diagnostic and therapeutic

* Corresponding authors.
E-mail addresses: lihi.norbert@science.unideb.hu (N. Lihi), kalman.ferenc@science.unideb.hu (F.K. Kálmán).
[1] These authors contributed equally.

https://doi.org/10.1016/j.ijpharm.2022.122527
Received 26 October 2022; Received in revised form 15 December 2022; Accepted 17 December 2022
Available online 23 December 2022

applications of other copper isotopes have attracted considerable attention in nuclear medicine and radiochemistry.(Dong et al., 2020) Among the Cu isotopes that are suitable for *in vivo* molecular imaging applications (^{60}Cu ($t_{1/2}$ = 23.7 min, β^+), ^{61}Cu ($t_{1/2}$ = 3.33 h), ^{62}Cu ($t_{1/2}$ = 9.67 min, β^+), and ^{64}Cu ($t_{1/2}$ = 12.70 h, β^+ and β^-)), the cyclotron produced ^{61}Cu with its long half-life and advantageous physical parameters (β^+: 1159 keV; γ: 511 keV) is suitable for PET imaging of slower processes, moreover, permits extended imaging and can also be transported (as it is happening frequently with FDG (fluorodeoxyglucose)) to distant PET imaging clinical centers where cyclotron is not available. (Boschi et al., 2018; Williams et al., 2005) In addition, its production is less expensive than that of several positron emitters.

In the last decades, considerable effort has been devoted to design and synthesize appropriate chelators which form highly stable and extremely inert complexes with Cu(II). These rigid and structurally constrained ligands are mostly the derivatives of 12-membered cyclen (1,4,7,10-tetraazacyclododecane) and 14-membered cyclam (1,4,8,11-tetraazacyclotetradecane) macrocycles containing alkane-bridge (located between two opposing nitrogen atoms) in their skeleton. (Weisman et al., 1996, 1990) This modification on the ligand backbone resulted in extremely high inertness of the Cu(II) complexes against H^+- or OH^- assisted dissociations.(Heroux et al., 2007; Hubin et al., 1998) Although, the inertness of the cross-bridged Cu(II) chelates is remarkable, their complexation reactions are immensely slow in mild conditions, therefore, their synthesis frequently requires harsh circumstances (e.g. organic solvents, high temperature, long reaction time etc.). (Hubin, 2003) Obviously, the high thermodynamic stability and inertness, the fast complex formation(Ferdani et al., 2012) as well as the resistance to reduction(Woodin et al., 2005) are all important parameters but the most crucial point is to find the reasonable balance between these features for the widespread application, especially in the work with short-lived radioisotopes. For the resolution of this issue, the CB-15aneN$_5$ ligand family(Shircliff et al., 2020; Wallace et al., 1995) provides an appropriate coordination environment for copper(II). Based on our previous work,(Csupász et al., 2022) the Cu(II) complexes of CB-15aneN$_5$ and its bifunctional derivative – *p*NO$_2$Bn-CB-15aneN$_5$ – designed for functionalization with biovectors (e.g. NAPamide), possess high thermodynamic stability, fast complex formation reaction and appropriate inertness for radiotheragnostic (combining therapeutics with diagnostics)(Jadvar et al., 2018) purposes. As it was presented, the formation of [[^{61}Cu]Cu(*p*NO$_2$Bn-CB-15aneN$_5$)]$^{2+}$ complex was fast with ^{61}Cu(II) isotope, showed successful (100 %) labeling at 10 μM ligand concentration and exhibited suitable serum stability for *in vivo* application as diagnostic agent.

Based on the promising results obtained for the [[^{61}Cu]Cu(*p*NO$_2$Bn-CB-15aneN$_5$)]$^{2+}$ complex,(Csupász et al., 2022) we aimed to synthetize novel radiopharmacon, [^{61}Cu]Cu-KFTG-NAPamide, that combines the advantageous properties of ^{61}Cu(II) isotope (i.e. its easy and inexpensive production in cyclotron from zinc, its good physical parameters such as decay half-life, $t_{1/2}$ = 3.3 h) and the excellent melanoma specificity of the NAPamide protein. This radioagent could provide a good alternative for rapid and inexpensive melanoma diagnostics in several cases due to its high affinity to melanoma tumors.

Since, the reduction of the NO$_2$ group to the corresponding NH$_2$ function is not a trivial task, a slight modification on the synthetic procedure was accomplished and instead of the *para*-nitrobenzyl moiety, the *para*-methyl-benzoic acid has been used as a linker between the ligand and the NAPamide protein yielding a new bifunctional chelator the *p*Bna-CB-15aneN$_5$ (Scheme 1), hereinafter mentioned as KFTG ligand. The incorporation of the *para*-methyl-benzoic acid into the ligand structure ensured the convenient conjugation through the formation of peptide bond between the carboxylic moiety of the KFTG ligand and the NH$_2$ group of the NAPamide.

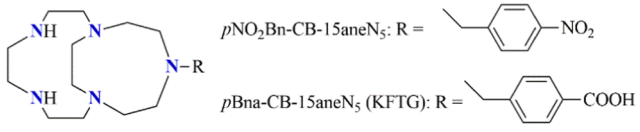

Scheme 1. The structure of the bifunctional ligands based on CB-15aneN$_5$ platform.

Although this modification on the structure of the chelator is not expected to cause significant deviation in the physico-chemical properties of the ligand and its Cu(II) complex (since, neither the *para*-nitrobenzyl, nor the *para*-methyl-benzoic acid moiety coordinate to the Cu(II) ion due to steric effect), the formation and dissociation rates of the [Cu(KFTG)]$^+$ complex as well as its superoxide dismutase (SOD) activity were determined. The structure of the complex has been examined by density functional theory method (DFT) and a thorough *in vivo* investigation on B16-F10 melanoma tumor-bearing C57BL/6J mouse model was carried out with the [^{61}Cu]Cu-KFTG-NAPamide as a potential diagnostic agent (time-dependent PET imaging and quantitative image analysis, organ distribution, log*P*, serum stability). Since [^{61}Cu]-based radiopharmacones have not been investigated on B16-F10 melanoma model for PET radioimaging so far, we demonstrate the advantages of the [^{61}Cu]Cu-KFTG-NAPamide for such purposes.

2. Materials and methods

The highest analytical grade chemicals were used for the experiments without further purification. Complexometric titrations were carried out with standardized Na_2H_2EDTA (H_4EDTA: ethylenediaminetetraacetic acid) (Merck) solution in the presence of murexid indicator to determine the concentration of the $CuCl_2$ (Merck) stock solution for analytical measurements.

Resin-bound NAPamide [Ac-Nle-Asp(*t*Bu)-His(Trt)-(D-Phe)-Arg(Pbf)-Trp(Boc)-Gly-Lys-(Rink Amide MBHA resin)] was purchased from CASLO ApS (Lyngby, Denmark). All other reagents were purchased from Sigma-Aldrich. Mass spectra were recorded on a Waters Acquity UPLC Iclass system (Waters, Milford, MA, USA). For the HPLC (high pressure liquid chromatography) system, HPLC-MS (MS: mass spectrometry) grade acetonitrile (ACN) and deionized water (Milli-Q, 18.2 MΩ cm^{-1}, Merck, Kenilworth, NJ, USA) were used. Semipreparative RP HPLC and analytical radio-HPLC were conducted using a Waters LC Module 1 HPLC and a Waters 2695 Alliance HPLC system connected to a UV detector and the ATOMKI 120 CsI scintillation detector. Semipreparative RP HPLC (RP: reversed phase) was performed using a Luna C18 10 μm (250 × 10 mm) column; solvent A: 0.1 % HCOOH; solvent B: ACN. Analytical HPLC was performed using a Luna C18 3 μm (150 × 4.6 mm) column, solvent A: oxalic acid (c = 0.01 M, pH = 3); solvent B: acetonitrile.

2.1. Synthesis of the ligands

Commercial reagents/solvents purchased from Sigma-Aldrich (St. Louis, MO, USA), Merck KGaA (Darmstadt, Germany) and Tokyo Chemical Industry (Tokyo, Japan) were used without further purification. The microwave activation was accomplished by a CEM Microwave Synthesis System (Discover-S #908860) including an Explorer 48 #909480 autosampler. The synthetic reactions were followed by using a Waters Alliance 2690 HPLC unit equipped with Waters 996 PDA detector, and a Phenomenex C18(2) 150*4.6 mm 3 μm column (Table S1 and S3). The preparative HPLC separations were carried out with a YL9100 HPLC system (Korea) equipped with YL9101S degasser, YL9110S pump, YL9120S UV/VIS detector, Phenomenex Luna Prep C18 (2) 100A 250x21.20 mm 10 μm 00G-4324-P0 column and Sigma-Aldrich CHROMASOLV® Plus solvents (Table S2). The NMR (nuclear magnetic resonance) measurements were carried out with *Bruker* DRX *360 MHz* and *Bruker Avance I 400 MHz* spectrometers using deuterated solvents. Mass spectra were recorded on a maXis II UHR ESI-QTOF MS Bruker instrument in the Laboratory of Instrumental Analysis, Department of

Inorganic and Analytical Chemistry at the University of Debrecen. The purity of the final products (KFTG and *bis*(Boc)-KFTG) was > 98.0 % determined by reverse-phase HPLC with UV − Vis detection at 220 and 260 nm.

***Tert*-butyl-4-((4,7-di(tosyl)-1,4,7,10,13-pentaazabicyclo [8.5.2] heptadecan-13-yl)-methyl)benzoate:** 4,7-Di(tosyl)-1,4,7,10,13-pentaazabicyclo[8.5.2]heptadecane (1.0 g, 1.82 mmol, 1.0 eq.) was measured into a flask and dissolved in 100 mL dry acetonitrile. K_2CO_3 (500 mg, 3.64 mmol, 2.0 eq.) was suspended into the solution. The flask was connected to a condenser and the mixture was heated to 60 °C. The *tert*-butyl-4-(bromomethyl)-benzoate (0.495 g, 1.82 mmol, 1.0 eq.) was dissolved in 100 mL dry acetonitrile and introduced into a dropping funnel which was connected to the flask. This mixture was added dropwise slowly to the hot reaction mixture which was stirred for 2 days. (The reaction was followed by analytical HPLC.) After completion of the reaction, the hot mixture was filtered through a G4 glass filter and the solvent was removed from the filtrate under reduced pressure. The product was white powder (749 mg, 56 % yield) and used in the subsequent step without further purification.

4-(1,4,7,10,13-pentaazabicyclo [8.5.2] heptadecan-13-yl) methyl)benzoic acid (KFTG): *tert*-butyl-4-((4,7-di(tosyl)-1,4,7,10,13-pentaazabicyclo[8.5.2]heptadecan-13-yl)methyl)benzoate (400 mg, 0.54 mmol, 1.0 eq.) was dissolved in 2.00 mL concentrated sulfuric acid. The reaction was performed in microwave reactor (120 °C, 15 W, 10 min.), and after then it was cooled to near 0 °C. After pouring the cold mixture into 100 mL cold diethyl-ether, a brown precipitate appeared. The acidic ether was decanted from the solid, which was dissolved in 5 mL of distilled water after the decantation. The pH of this solution was adjusted to near 4.0 and the product was purified by preparative HPLC, which was a yellow solid (105 mg, 52 % yield). ^{1}H NMR (360 MHz, D_2O): δ (ppm) 8.37 (2H, d, J = 8.0 Hz, aromatics), 7.79 (2H, d, J = 8.0 Hz, aromatics), 4.23 (2H, s, –CH_2-), 3.55 (4H, m, –CH_2-), 3.51–3.33 (8H, m, –CH_2-), 3.30–3.22 (10*H*, m, –CH_2-) 3.19 (2H, m, –CH_2-). ^{13}C NMR (90 MHz, CD_3CN): δ (ppm) 169.2 (1C, *C*═O), 141.9, 129.6 (2 × 1C, *Cq*-aromatics), 130.0, 129.8, (2 × 2C, aromatics), 58.0, 52.2, 50.0, 48.0, 46.6, 42.9, 41.7 (1 × 1C + 6 × 2C, –*C*H$_2$-). ESI-MS (electrospray ionization mass spectrometry) (*m/z*, positive mode): $[M + H]^+_{calc.}$: 376.2707, $[M + H]^+_{found}$: 376.2706 (Figure S1-S4).

4-((4,7-bis(*tert*-butoxycarbonyl)-1,4,7,10,13-pentaazabicyclo [8.5.2] heptadecan-13-yl)methyl)benzoic acid (*bis*(Boc)-KFTG): KFTG (140 mg, 0.373 mmol, 1.0 eq.) was dissolved in 20.0 mL THF (tetrahydrofuran) and triethylamine (530 µL, 3.73 mmol, 10.0 eq.) was added to this mixture. This mixture was cool down in an ice bath to near 0 °C and the solution of di-*tert*-butyl dicarbonate (370 mg, 1.12 mmol, 3.0 eq) in THF (10 mL) was added to the reaction, which was stirred overnight at room temperature. The pH of this solution was adjusted to near 7 and the compound was purified by preparative HPLC method. The product was a white solid (105 mg, 52 % yield). ^{1}H NMR (400 MHz, D_2O/CD_3CN): δ (ppm) 8.57 (2H, d, J = 8.2 Hz, aromatics), 8.00 (2H, d, J = 8.2 Hz, aromatics), 4.48 (2H, s, –CH_2-), 4.19–3.33 (24H, *m*, –CH_2-), 2.03 (18H, m, –CH_3). ^{13}C NMR (90 MHz, D_2O): δ (ppm) 168.7 (1C, *C*═O), 156.8 (2C, *C*═O), 140.5, 132.0 (2C, *C*q aromatics), 130.5, 130,1, (2 × 2C, aromatics), 81.4, (2C, *C*q, -tBu), 58.3, 56.7, 51.3, 49.6, 47.3, 44.6, (1 × 1C + 6 × 2C, –*C*H$_2$-); 27.9 (2 × 3C, –*C*H$_3$, -tBu). ESI-MS (*m/z*, positive mode): $[M + H]^+_{calc.}$: 576.3756, $[M + H]^+_{found}$: 576.3756 (Figure S5-S8).

2.2. Kinetic experiments

The formation rate of the $[Cu(KFTG)]^+$ complex was studied at 25 °C and 0.15 M NaCl ionic strength in the presence of 10 times excess of ligand to ensure pseudo-first order conditions. The absorbance change was monitored at 285 nm with a Cary 100 Bio UV–vis spectrophotometer. The Cu(II) concentrations in the reactions were 0.1 mM. The formation reactions were carried out in the pH range 3.4–4.6 using DMP buffer (1,4-dimethylpiperazine, pK_a = 4.2) in 50 mM concentration.

The inertness of the complexes was investigated in 5.0 M HCl at 50 °C. The concentration of the complex were 0.1 mM.

2.3. Plasma stability

50 µL sample of [^{61}Cu]Cu-KFTG-NAPamide was mixed with 500 µL human plasma and kept at 37 °C for six hours. Samples were taken and separated on ITLC-SG (instant thin layer chromatography - silica-gel) stripes, eluted with ammonium acetate – methanol 1:1.

2.4. DFT calculation

The geometry of the $[Cu(KFTG)]^+$ complex was optimized through the Gaussian 09 (Rev. E.01) software package at DFT level of theory. (Frisch et al., 2009) The hybrid Becke three-parameter B3P86 functional was used in this calculation.(Becke, 1993) The relativistic small-core ECPs SDD and LANL2DZ with the corresponding valence basis sets were employed on the copper(II) and the triple-ζ *def2*-TZVP basis set for the main group elements.(Bühl and Kabrede, 2006; Dolg et al., 1987; Hay and Wadt, 1985) The effect of the solvent was take into account adopting the Polarizable Continuum Model (PCM) for water.(Tomasi et al., 2005) Single point calculations were carried out for the ground state geometry at the same level of theory which represented true minima on the potential energy surface. Cartesian coordinates of the copper(II) complex were generated by EsiGen(Rodríguez-Guerra Pedregal et al., 2018) software while Chimera (1.15)(Pettersen et al., 2004) was used to visualize the complex.

2.5. Superoxide dismutase (SOD) activity measurement

The dismutation reaction between the superoxide anion and $[Cu(KFTG)]^+$ complex was quantitatively studied using the xanthine / xanthine oxidase / NBT assay. The assay was carried out in phosphate buffer (pH = 7.6; c = 50 mM) containing 45 µM NBT and 200 µM xanthine. The reaction was initiated by adding an appropriate amount of xanthine oxidase to set a ca. 0.020 min^{-1} rate of absorbance increase at 560 nm. First, the reaction was monitored in a control sample without the addition of the complex. In the test samples, the reaction was started, let to run for 3 min, then the $[Cu(KFTG)]^+$ complex was added, and the system was monitored further for 4 min. The original and the altered rates of the absorbance increase were estimated by fitting the appropriate parts of the kinetic curves with linear (zeroth order rate) functions. The calculations for estimating the inhibition parameters were performed using the conventional method reported in the literature. (Zhou and Prognon, 2006) The SOD activity of the complex is expressed in copper-concentration equivalent IC_{50} values.

2.6. Labeling experiments, general procedures

Synthesis of KFTG-NAPamide. A solution of HBTU (7 mg, 0.018 mmol) in anhydrous DMF (dimethylformamide) (1 mL), DIPEA (3 µL, 0.017 mmol) and a solution of *bis*(Boc)-KFTG (5 mg, 0.007 mmol) in anhydrous DMF (1 mL) were added to the protected, resin-bounded NAPamide [Ac-Nle-Asp(*t*Bu)-His(Trt)-(D-Phe)-Arg(Pbf)-Trp(Boc)-Gly-Lys-(Rink Amide MBHA resin)] (30 mg, 0.0045 mmol). The mixture was shaken for 3 h at RT (room temperature) then the resin was washed with anhydrous DMF. The acidic hydrolysis was performed in 95 % TFA (1 mL). After shaking for 6 h the TFA was evaporated, and the crude peptide derivative was purified by HPLC. For semipreparative RP-HPLC, a Luna C18(2) 100 Å10 µm (250 × 10 mm) column was eluted at a flow rate of 4 mL•min^{-1} using the following solvents: solvent A: 0.1 % HCOOH solvent, B: 95 % acetonitrile, gradient: 0 min: 100 % A, 2 min: 100 % A, 32 min: 100 % B, 40 min 100 % B. The product was collected between 15 and 16 min. After lyophilization, KFTG-NAPamide was obtained as a white powder (1.3 mg, yield: 20 %). HRMS ESI (electrospray ionization high-resolution mass spectrometry) calc. for:

$C_{72}H_{105}N_{21}O_{12}$, 728.9204 $[M + H]^{2+}$ and 486.2829 $[M + H]^{3+}$, Found: 728.9174 $[M + H]^{2+}$, 486.2832 $[M + H]^{3+}$.

2.7. Isotope production

^{61}Cu was produced from natural zinc foil (Sigma Aldrich, 99.999 % purity, 10x10x0,1 mm size, 0.25 mm thickness) irradiated by 15.5 MeV proton beam (30 min., 20 μA) in a GE PETtrace cyclotron. Typical ^{61}Cu activity after separation from gallium isotopes was 250–330 MBq. The irradiated target material was dissolved in 2 mL of HNO_3 ($c = 7$ M) and mixed with 5 mL of ammonium formate solution ($c = 2.5$ M) to set the pH to 2. The solution was loaded to a small CU resin column (6 × 9 mm). After washing with 10 mL water, the trapped activity was eluted with 0.5 mL of 7 M HCl and evaporated to dryness. The ^{61}Cu was dissolved in 0.01 M HCl or HEPES buffer (4-(2-hydroxyethyl)-1-piperazineethanesulfonic acid, pH = 7).

2.8. [^{61}Cu]-labeling experiments

5 μL aliquots of solution containing 1 mg/mL KFTG-NAPamide was added to approximately 100 MBq ^{61}Cu in 50 μL 1 M HEPES buffer (pH = 7) and heated to 95 °C for 15 min in a closed Eppendorf tube. The solution was diluted with 1 mL water, and loaded to a Waters light C18 SPE cartridge. After washing with water, the labelled peptide was eluted with 500 μL saline-ethanol 1:1 mixture. The solution was evaporated to near dryness with heating in nitrogen stream and diluted with saline solution. Radiochemical purity was determined with radio-TLC on ITLC stripes, eluted with ammonium acetate – methanol 1:1. The molar activity of the labelled peptide was 52–58 MBq/nmol.

2.9. Determination of LogP

A sample of [^{61}Cu]Cu-KFTG-NAPamide in HEPES buffer (pH = 7) was added to 0.5 mL water and 0.5 mL octanol in an Eppendorf vial. The vial was vortexed for several minutes and left to stand until phase separation. 50 μL aliquots were taken from the phases and counted with a gamma counter.

2.10. In vitro cellular uptake and efflux studies

B16-F10 mouse and amelanotic A375 human melanoma cells (purchased from the American Type Culture Collection (ATCC)) were grown as monolayer in Dulbecco's Modified Eagle's medium (DMEM, GIBCO Life Technologies) supplemented with 10 % Fetal Bovine Serum (FBS, GIBCO Life technologies), 1 % (v/v) MEM amino acid, vitamins and antibiotic-antimicotic solution (Sigma-Aldrich). Cells were cultured under standard conditions at 5 % CO_2, and 37 °C.

For the *in vitro* experiments B16-F10 and A375 cells were trypsinized, washed and resuspended in cell culture medium. Cells were aliquoted in test tubes at a cell concentration of 1x10^6 ml^{-1}, and incubated for 30, 60, 90 and 180 min after the addition of 0.37 MBq [^{61}Cu]Cu-KFTG-NAPamide at 37 °C; then samples were washed 3 times with ice-cold PBS and the radioactivity uptake was measured with gamma counter (Hewlett Packard Cobra II Autogama Gamma Counter, USA). For the efflux studies melanoma cells were incubated in the presence of [^{61}Cu]Cu-KFTG-NAPamide (0.37 MBq at 37 °C) for 30, 60, 90 and 180 min. After the incubation time cells were washed with PBS containing 1 mM glucose (gl-PBS) at room temperature. Subsequent centrifugation the supernatant was removed and the cells were resuspended in 2 mL gl-PBS and further incubated for 10 min at 37 °C without the radioligand. The efflux was terminated by the addition of ice-cold PBS, cells were then washed twice with ice cold PBS and the radioactivity was measured by using a calibrated gamma-counter (Hewlett Packard Cobra II Autogama Gamma Counter, USA). The uptake of [^{61}Cu]Cu-KFTG-NAPamide was expressed as percentage of the total radioactivity of radiotracers added to the cells (ID%/10^6 cells). Each experiment was performed in triplicate and the displayed data represents the means of at least three independent experiments.

2.11. In vivo tumor model

C57BL/6J mice (12-week-old, female, n = 30; Charles River Laboratories) were housed under sterile conditions in IVC cages (individually ventilated cage) at a temperature of 26 ± 2 °C with 55 ± 10 % humidity and artificial lighting with a circadian cycle of 12 h. Semi-synthetic diet (Akronom ltd., Budapest, Hungary) and drinking water were available *ad libitum* to all the animals. Laboratory animals were kept and treated in compliance with all applicable sections of the Hungarian Laws and regulations of the European Union. For the induction of MC1-R positive melanoma tumors C57BL/6J mice were injected with 1x10^6 B16-F10 tumor cells in 100 μL saline subcutaneously into the left shoulder area. In vivo and *ex vivo* experiments were carried out 8 ± 1 days after tumor cell inoculation at the tumor volume of 120 ± 10 mm^3.

2.12. In vivo PET imaging

For *in vivo* imaging studies B16-F10 tumor-bearing mice were injected intravenously with 10.3 ± 0.3 MBq of [^{61}Cu]Cu-KFTG-NAPamide *via* the lateral tail vein, and dynamic PET scans were performed under 1.5 % isoflurane (Forane, AbbVie) anesthesia (Tec3 Isoflurane Vaporizer, Eickemeyer Veterinary Equipment, UK) using the preclinical MiniPET-II imaging device (University of Debrecen, Faculty of Medicine, Department of Medical Imaging, Division of Nuclear Medicine and Translational Imaging). Reconstructed images were analyzed using the BrainCad image analysis software. Ellipsoidal 3-dimensional Volumes of Interest (VOIs) were manually drawn around the edge of the tissue or organ activity by visual inspection. Radiotracer uptake was expressed in terms of standardized uptake values (SUVs). SUV was calculated as follows: SUV = [VOI activity (Bq/ml)]/[injected activity (Bq)/animal weight (g)], assuming a density of 1 g/mL. Tumor-to-muscle (T/M) ratios were calculated from the activity of tumor and background (muscle).

2.13. Ex vivo biodistribution studies

8 ± 1 days after tumor cell inoculation B16-F10 tumor-bearing mice were injected intravenously with 10.3 ± 0.3 MBq of [^{61}Cu]Cu-KFTG-NAPamide, and after 30-, 60-, 90- and 180-min incubation time mice were euthanized with 5 % Forane. Tissue samples were taken from selected organs and the weight, and the radioactivity of the samples were measured with calibrated gamma counter (Hewlett Packard Cobra II Autogama Gamma Counter, USA) and the uptake was expressed as % ID/g tissue.

Statistical analysis. Significance was calculated by two-way ANOVA, Student's *t*-test (two-tailed) and Mann-Whitney *U* test using the MedCalc 18.5 software package (MedCalc Software, Mariakerke, Belgium). The significance level was set at p less than 0.05 unless otherwise indicated. Data are presented as mean ± SD of at least three independent experiments.

The ethical approval for animal experiments was given by Animal Welfare Committee of University of Debrecen (16/2020/DEMÁB). Study design and the animal experiments were in accordance with the ARRIVE guideline.(Percie du Sert et al., 2020).

3. Results and discussion

3.1. Synthesis of the ligands

The KFTG ligand has been synthesized according to the procedure published previously(Csupász et al., 2022) using *tert*-butyl-4-(bromomethyl)benzoate instead of 4-nitrobenzyl bromide to settle the bifunctional character of the ligand. In order to avoid the amidation of the

secondary amine nitrogen atoms in the functionalization reaction carried out with NAPamide, *tert*-butyloxycarbonyl protecting groups (Boc) were used. The detailed characterization of the new ligands (Figure S1-S8 and Table S1-S3) and the synthetic procedures are provided in the SI. The synthesis of KFTG-NAPamide (Figure S1) was performed by standard amide conjugation, thus *bis*(Boc)-KFTG bifunctional chelator was coupled via an active ester to the free amine group of the lysine unit of the resin-bound NAPamid peptide using HBTU (hexafluorophosphate benzotriazole tetramethyl uronium) and DIPEA (N,*N*-diisopropylethylamine) activation strategy. Then, the obtained resin-bound peptide derivative was deprotected and cleaved from the resin with acidic hydrolysis using 95 % TFA (trifluoroacetic acid). The crude peptide with the KFTG moiety was purified by semipreparative RP-HPLC. The chelator-conjugated NAPamide was identified by HRMS SI.

3.2. Formation and dissociation kinetic studies

The fast complexation of the short-lived radioisotopes is essential to minimalize radioactive decay of the agents for preserving the diagnostic and therapeutic effects. As it was pointed out, the chelation of the Cu(II) by the rigidified tetraaza-macrocycles often requires high temperature and organic solvents which is obviously time and resource consuming.

First, the formation of the $[Cu(KFTG)]^+$ complex was studied according to the method published previously.(Csupász et al., 2022) The complexation reactions were carried out in the presence of ligand excess (×10) to ensure pseudo-first-order condition at 25 °C (Fig. 1). Under these conditions the rate of the complex formation can be given by the rate equation $d[CuL]_t/dt = k_{obs}[Cu(II)]$, where $[CuL]_t$ is the total concentration of the chelate.

As presented in Fig. 1, the rate constants (k_{obs}) obtained at different pH values are directly proportional to the increase of $[OH^-]$ for the $[Cu(KFTG)]^+$ complex and the formation rate of the complex exhibits second-order dependence on OH^- concentration. Thus, the pseudo-first-order rate constants for the complex formation can be expressed as follow:

$$k_{obs} = k_1[OH^-] + k_2[OH^-]^2 \quad (1)$$

where k_1 and k_2 are the rate constants characterizing the transformation of the intermediate to product assisted by the OH^-. The mechanism of the reaction was not investigated in detail. The fitting of the k_{obs} rate constants to equation (1) yields $k_1 = (1.2 \pm 0.1) \times 10^6$ $M^{-1}s^{-1}$ and $k_2 = (3.3 \pm 0.5) \times 10^{15}$ $M^{-2}s^{-1}$. For comparison, the $t_{1/2}$ ($t_{1/2} = \ln 2/k_{calc}$) of the formation reaction was calculated to be 155 s at pH = 5.0 which is similar to that obtained for the $[Cu(pNO_2Bn\text{-}CB\text{-}15aneN_5)]^{2+}$ complex, $t_{1/2} = 133$ s.(Csupász et al., 2022) The results show that the KFTG ligand forms Cu(II) complex in less than 20 min (7 times $t_{1/2}$) at pH 5.0 and 25 °C.

Since the dissociation of rigidified Cu(II) complexes is extremely slow under mild circumstances, their inertness is usually investigated in harsh conditions such as high acid concentration and elevated temperature.(Shircliff et al., 2020) Detailed characterization of the different dissociation pathways (e.g. proton- and metal-assisted dissociation) is challenging or even impossible in these systems, therefore the dechelation reactions of the complexes are monitored at high acid concentration (e.g. 5 M HCl) and elevated temperature (50 or 90 °C). Since the high H^+ concentration ensures the pseudo-first order conditions for this reaction, the obtained k_{obs} values can be handled as pseudo-first order rate constants and easily converted to dissociation half-lives for comparison. The inertness of the $[Cu(KFTG)]^+$ complex has been studied in 5.0 M HCl at 50 °C. The $t_{1/2}$ value calculated for the dissociation of $[Cu(KFTG)]^+$ found to be 2.0(1) hours which is in good agreement with that determined for the $[Cu(pNO_2Bn\text{-}CB\text{-}15aneN_5)]^{2+}$ complex (2.3 h).(Csupász et al., 2022) The results indicate that the alternation of the nitrobenzil moiety to benzoic acid does not lead to significant differences either in the formation or in the dissociation features of the Cu(II) complex. For the sake of clarity, it should also be mentioned that the physico-chemical features of the chelators slightly alter upon the functionalization, which means that these values determined for the $[Cu(KFTG)]^+$ complex are only good approximations to describe the properties of the radiopharmacon. However, the inertness of our complex is less than that of many cross-bridged Cu(II) complexes,(Anderson et al., 2008) the *in vitro* and *in vivo* experiments performed with $[^{61}Cu(KFTG)]$-NAPamide confirmed that the inertness of the agent is high enough for ^{61}Cu-based PET diagnostic applications (less than 4 % dissociation in blood plasma at 37 °C during 6 h, Figure S9).

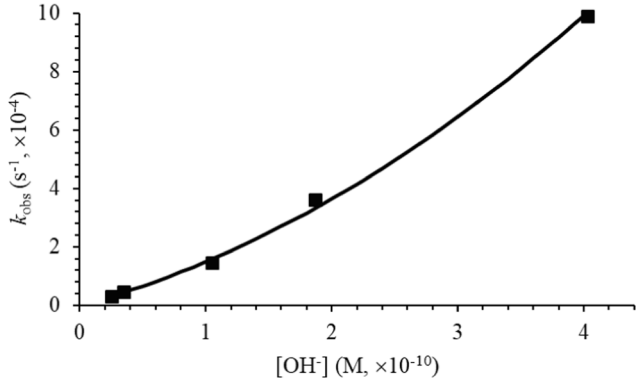

Fig. 1. Plot of the first-order rate constants (k_{obs}) as a function of $[OH^-]$ for the formation of $[Cu(KFTG)]^+$ (0.15 M NaCl, 25 °C).

3.3. DFT calculations and SOD activity

In order to explore the structure of the $[Cu(KFTG)]^+$ complex, DFT calculations were carried out. According to the results obtained for the $[Cu(pNO_2Bn\text{-}CB\text{-}15aneN_5)]^{2+}$ complex, the ligand coordinates to the copper(II) via the 5 nitrogen donor atoms yielding a pentacoordinated copper(II) species. DFT optimized structure is shown in Fig. 2 and the corresponding Cartesian coordinates are reported in the SI (Table S4). An average equatorial bond length of 2.016 Å and an apical of 2.315 Å which is in good agreement with those obtained for the $[Cu(pNO_2Bn\text{-}CB\text{-}15aneN_5)]^{2+}$ complex. The index of trigonality, τ, was calculated to be 0.45 which implies that the coordination polyhedron falls into the geometry between the bipyramidal and square-pyramidal structures.

The *in vivo* stability of a Cu(II)-based agent depends not only on the

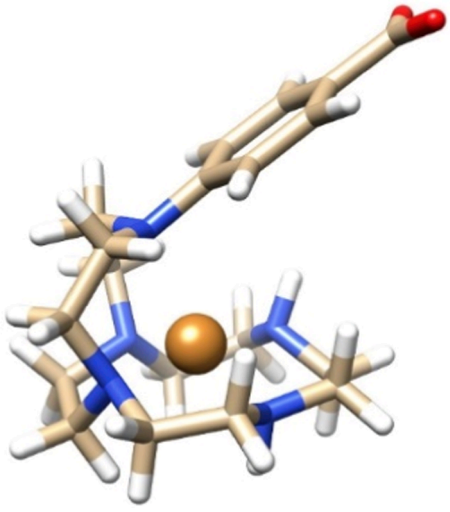

Fig. 2. DFT optimized structure of $[Cu(KFTG)]^+$ complex at B3P86 with *def2*-TZVP basis set for main group elements and LANL2DZ for copper(II). The PCM method was used to take into account the effect of the solvent (water).

resistance of the chelate against the dissociation but also on the redox stability of the metal complex. The reduction of the Cu(II) to Cu(I) provokes the dissociation of the chelate (due to the different coordination properties of the two ions), which leads to the loss of the diagnostic effect. Interestingly, the reaction between reactive oxygen species (ROS) and Cu(II) complexes could induce the dechelation, since the reduction of the central metal ion occurs in the first step of the metal assisted dismutation of superoxide radicals. If the intermediate complex is very labile as it can be envisioned for the copper(I) complexes, the dissociation of that may overtake the oxidation step promoting the liberation of the radioisotope.

For this reason, the antioxidant capability of the pristine [Cu(KFTG)]$^{+}$ complex was tested via the xanthine/xanthine oxidase/NBT system. The inhibition percentage at each concentration was calculated and the results are shown in the SI. The IC_{50} value of the [Cu(KFTG)]$^{+}$ complex was found to be 2.3 ± 0.3 μM at physiological pH, consequently, the copper(II) complex exhibits moderate SOD activity (Figure S10).

3.4. Labeling experiments

(KFTG)-NAPamide was quantitatively labelled in approximately 30 μM concentration level with ^{61}Cu in pH = 7 HEPES buffer at 95 °C for 15 min. The labelled peptide was purified with solid phase extraction and used in animal experiments. The octanol/water partition coefficient was found to be –1.99, showing slightly lower hydrophilicity than the ^{68}Ga or ^{44}Sc labelled DOTA (1,4,7,10-tetraazacyclododecane-1,4,7,10-tetrayl)tetraacetic acid) analogs (−3.5 and −3.3, respectively).(Nagy et al., 2017) Plasma stability was determined in human plasma. Radiochemical purity did not change significantly (less than 4 % decrease) during two half-lives (6 h).

3.5. In vitro accumulation studies

The accumulation of [^{61}Cu]Cu-KFTG-NAPamide in the MC1-R positive B16-F10 melanoma cells were significantly higher (p less than 0.01) than in amelanotic A375 cells at each investigated time point (Fig. 3) confirming the receptor specificity of the [^{61}Cu]Cu-KFTG-NAPamide probe. In the washout (efflux) investigations, melanoma cells were first loaded with [^{61}Cu]Cu-KFTG-NAPamide, and after the incubation time and washing rounds, B16-F10 and A375 cells were incubated without radioactivity for additional 10 min. In efflux studies the MC1-R positive B16-F10 cells showed significantly ($p \leq 0.01$) higher [^{61}Cu]Cu-KFTG-NAPamide content at each time point than the receptor negative A375 cell line (Fig. 3). No significant difference (at $p < 0.05$) was found between the baseline and the post-efflux radioactivity concentrations in the examined cells (Fig. 3).

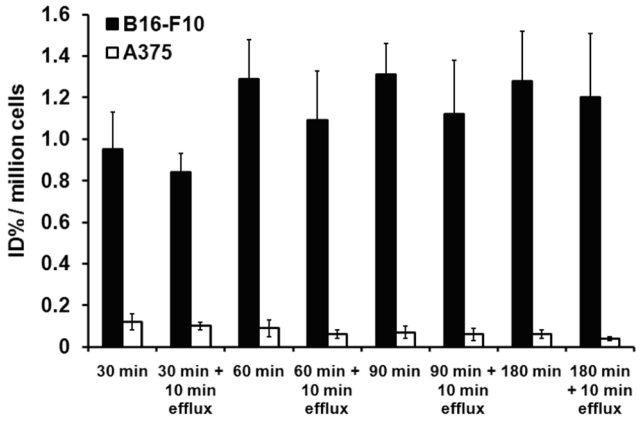

Fig. 3. Assessment of cellular uptake and efflux studies of the MC1-R specific [^{61}Cu]Cu-KFTG-NAPamide. Comparative study of time dependent [^{61}Cu]Cu-KFTG-NAPamide accumulation and washout (efflux) results of B16-F10 and A375 cells. Data shown as mean ± SD. [^{61}Cu]Cu-KFTG-NAPamide accumulation in 10^6 cells was expressed as the percentage of the incubating dose (ID%).

3.6. In vivo tumor targeting experiments

The tumor targeting potential of [^{61}Cu]Cu-KFTG-NAPamide was assessed by *in vivo* preclinical PET imaging and *ex vivo* biodistribution studies using MC1-R receptor positive B16-F10 mouse melanoma tumor model. After the qualitative analysis of the decay-corrected PET images we found that the tumor was well identifiable at each investigated time point (Fig. 4 "A").

The quantitative SUV analysis showed remarkable radiopharmaceutical accumulation at 30 min post injection (SUVmean: 0.4 ± 0.1; SUVmax: 0.6 ± 0.1), which increased till 60 min (SUVmean: 0.7 ± 0.1; SUVmax: 1.3 ± 0.1), then no further significant increase was observed at 90 min (SUVmean: 0.8 ± 0.1; SUVmax: 1.3 ± 0.2) and 180 min (SUVmean: 0.8 ± 0.2; SUVmax: 1.3 ± 0.1) (Fig. 4 "B"). However, a sharp rise in the tumor-to-background (muscle) ratio (T/M) was observed as the accumulation of the [^{61}Cu]Cu-KFTG-NAPamide in the background decreased significantly with time (Fig. 4 "C", the experimental data are shown in Table S5). Previous *in vitro* and *in vivo* studies also reported that radiolabeled α-MSH analogs showed high uptake in B16 melanoma cells and high accumulation in B16-F10 tumors due to the significant MC1-R expression where the receptor binding capacity were calculated to be approximately 22,000 sites/cell.(Cheng et al., 2007a,b; Tafreshi

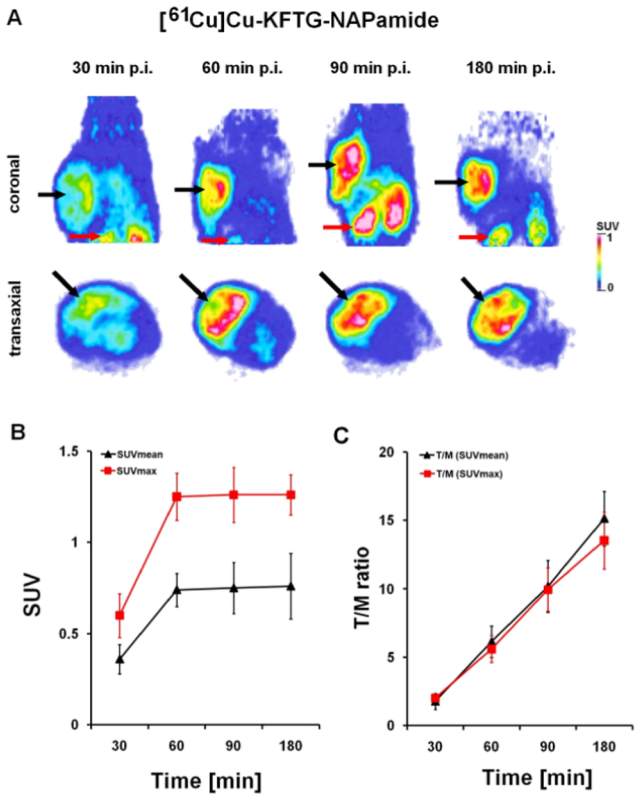

Fig. 4. In vivo PET imaging and quantitative image analysis of melanoma tumors using [^{61}Cu]Cu-labeled KFTG-NAPamide radiotracer. Representative transaxial (A) PET images of B16-F10 melanoma tumor-bearing C57BL/6J mouse 30, 60, 90 and 180 min after the intravenous injection of [^{61}Cu]Cu-KFTG-NAPamide. Quantitative SUV analysis of [^{61}Cu]Cu-KFTG-NAPamide accumulation in experimental melanoma tumors (B, C). Decay-corrected PET images and data were obtained 8 ± 1 days after tumor cell inoculation. n = 5 animals/time point. Black arrows: B16-F10 tumors, red arrows: kidneys. SUV: standardized uptake value. SUV values are presented as mean ± SD. T/M: tumor-to-muscle ratio.

et al., 2012) According to the previously described strong MC1-R positivity of B16-F10 tumors, we also found that the subcutaneously transplanted B16-F10 tumors were clearly detectable with excellent image contrast with high T/M ratios using the MC1-R specific [^{61}Cu]Cu-KFTG-NAPamide probe. This T/M ratio is higher than further [^{68}Ga]Ga-labeled α-melanocyte-stimulating hormone employed for B16F10 melanoma model and [^{64}Cu]Cu-NOTA-GGNle-CycMSH$_{hex}$(Zhang et al., 2017b) radiopharmacon tested on B16/F1 melanoma cells.(Guo and Miao, 2012) However, the %ID/g uptake of the tumor is lower than those observed for these radiopharmacons. However, it is important to highlight that the direct comparison between these radiopharmacon candidates is not trivial since their building blocks and targets are somewhat different.

For the determination of the biodistribution of [^{61}Cu]Cu-KFTG-NAPamide *ex vivo* studies were performed at different time points (Fig. 5). After the quantitative analysis of the *ex vivo* %ID/g data we found that the uptake of [^{61}Cu]Cu-KFTG-NAPamide in all healthy organs decreased with time. According to the log*P* value (log*P* = –1.99), the kidneys and the urine showed the highest radiotracer accumulation confirming that the complex is excreted from the animal mainly through the urinary system. Relatively high liver accumulation (approximately 6–9 %ID/g) was observed at each investigated time point. Similar results were found by Cheng and co-workers, where significant radioactivity uptake was also observed in the liver than in the case of [^{61}Cu]Cu-KFTG-NAPamide. A reasonable explanation for this phenomenon may be the ^{61}Cu releasing due to the decomposition and transchelation in the blood and liver caused by the effect of peptidases.(Cheng et al., 2007a)

The *ex vivo* %ID/g data of the MC1-R positive B16-F10 tumors (Fig. 5 and Table 1) correlated well with the *in vivo* SUV analysis. Table 1 demonstrates that the uptake of [^{61}Cu]Cu-KFTG-NAPamide in the MC1-R receptor positive tumor reached the maximum at 60 min and then no further increase was observed. The comparison of the *in vivo* and *ex vivo* uptake values of the [^{61}Cu]Cu-KFTG-NAPamide with previously investigated radiolabeled NAPamide radiotracers leads to the conclusion that the [^{61}Cu]Cu-KFTG-NAPamide yields approximately 3–5-fold higher accumulation in B16-F10 tumors than that of the ^{68}Ga- and ^{44}Sc-labeled DOTA-NAPamide derivatives after the same incubation time.(Nagy et al., 2017) Moreover, approximately 1.5-fold higher %ID/g value was observed by using [^{61}Cu]Cu-KFTG-NAPamide (60 min %ID/g: 7.6 ± 1.7) than that of [^{64}Cu]Cu-DOTA-NAPamide after *ex vivo* tumor uptake analysis (60 min %ID/g: 3.7 ± 0.3).(Zhen Cheng et al., 2007; Zhang et al., 2017a).

Table 1
Ex vivo biodistribution data for [^{61}Cu]Cu-KFTG-NAPamide. Quantitative analysis of ex vivo biodistribution data (n = 5 animals/time point) 30, 60, 90 and 180 min after intravenous injection of the radiotracer. %ID/g values are presented as mean ± SD.

Tumor	[^{61}Cu]Cu-KFTG-NAPamide			
	30 min	60 min	90 min	180 min
B16-F10	5.2 ± 2.0	7.6 ± 1.7	7.4 ± 1.8	7.3 ± 1.0
B16-F10 T/M	6.1 ± 1.1**	22 ± 3**	52 ± 10**	315 ± 24**

4. Conclusion

As a result of this study, we propose the [^{61}Cu]Cu-KFTG-NAPamide complex as the first ^{61}Cu-based radiopharmaceutical in this field, for the non-invasive diagnosis of malignant melanoma by the highly sensitive PET imaging. The physico-chemical characterization of the pristine [Cu(KFTG)]$^+$ complex describes fast complex formation (less than 20 min at pH = 5.0 and 25 °C) and suitable high inertness ($t_{1/2}$ = 2.0 h at 50 °C in 5 M HCl) for the rigid chelate. The DFT calculations predicted a pentacoordinated copper(II) species possessing a 0.45 trigonality index, which means that the coordination polyhedron falls into the geometry between the bipyramidal and square-pyramidal structures. Furthermore, the [Cu(KFTG)]$^+$ chelate shows moderate SOD activity. In order to gain information on the plasma stability of the [^{61}Cu]Cu-KFTG-NAPamide, the dechelation of the agent was studied in human plasma resulted in less than 4 % loss of activity during 6 h. From the *in vivo* and *ex vivo* results one can conclude that the [^{61}Cu]Cu-KFTG-NAPamide radiotracer bounds to the MC1-R positive experimental melanoma tumors with high affinity, which was confirmed by the SUV and %ID/g values. In addition, due to the fast elimination from the background, and its excretion through the kidneys, the [^{61}Cu]Cu-KFTG-NAPamide results in an excellent image contrast, which greatly facilitates the evaluation of the PET images, thus the identification of MC1-R positive tumors. To the best of our knowledge, [^{61}Cu]-based radiopharmachones have not been reported so far, consequently we propose the [^{61}Cu]Cu-KFTG-NAPamide as the first [^{61}Cu]Cu candidates for PET radioimaging studied on B16-F10 melanoma model with excellent radiodiagnostic features.

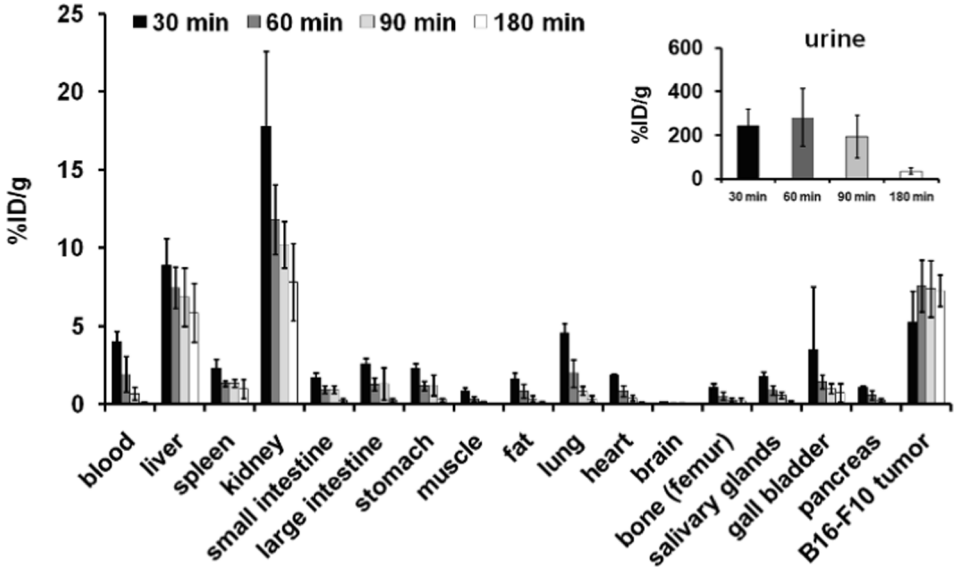

Fig. 5. *Ex vivo* biodistribution data for [^{61}Cu]Cu-KFTG-NAPamide. Quantitative analysis of *ex vivo* biodistribution data (n = 3 animals/time point) 30, 60, 90 and 180 min after intravenous injection of the radiotracer. %ID/g values are presented as mean ± SD.

Declaration of Competing Interest

The authors declare that they have no known competing financial interests or personal relationships that could have appeared to influence the work reported in this paper.

Data availability

Data will be made available on request.

Acknowledgements

The research was funded by the Hungarian National Research, Development and Innovation Office (FK-134551) project, the New National Excellence Program ÚNKP-21-5 and ÚNKP-22-5 (F. K. K.). F. K. K. acknowledges financial support of the János Bolyai Research Scholarship of the Hungarian Academy of Sciences. The authors are indebted to KIFÜ for awarding access to resource based in Hungary. The research was supported by the KDP-2021 program of the Ministry for Innovation and Technology from the source of the National Research, Development and Innovation Fund (Gy.T. and I. K-SZ.).

Appendix A. Supplementary data

Supplementary data to this article can be found online at https://doi.org/10.1016/j.ijpharm.2022.122527.

References

Ahmed, B., Qadir, M.I., Ghafoor, S., 2020. Malignant Melanoma: Skin Cancer-Diagnosis, Prevention, and Treatment. Crit. Rev. Eukaryot. Gene. Expr. 30, 291–297. https://doi.org/10.1615/CritRevEukaryotGeneExpr.2020028454.

Anderson, C.J., Wadas, T.J., Wong, E.H., Weisman, G.R., 2008. Cross-bridged macrocyclic chelators for stable complexation of copper radionuclides for PET imaging. Q. J. Nucl. Med. Mol. Imaging 52, 185–192.

Becke, A.D., 1993. Density-functional thermochemistry. III. The role of exact exchange. J. Chem. Phys. 98, 5648–5652. https://doi.org/10.1063/1.464913.

Boschi, A., Martini, P., Janevik-Ivanovska, E., Duatti, A., 2018. The emerging role of copper-64 radiopharmaceuticals as cancer theranostics. Drug. Discov. Today 23, 1489–1501. https://doi.org/10.1016/j.drudis.2018.04.002.

Bühl, M., Kabrede, H., 2006. Geometries of Transition-Metal Complexes from Density-Functional Theory. J. Chem. Theory. Comput. 2, 1282–1290. https://doi.org/10.1021/ct6001187.

Cheng, Z., Xiong, Z., Subbarayan, M., Chen, X., Gambhir, S.S., 2007a. ^{64} Cu-Labeled Alpha-Melanocyte-Stimulating Hormone Analog for MicroPET Imaging of Melanocortin 1 Receptor Expression. Bioconjugate. Chem. 18, 765–772. https://doi.org/10.1021/bc060306g.

Cheng, Z., Zhang, L., Graves, E., Xiong, Z., Dandekar, M., Chen, X., Gambhir, S.S., 2007b. Small-Animal PET of Melanocortin 1 Receptor Expression Using a 18F-Labeled -Melanocyte-Stimulating Hormone Analog. J. Nucl. Med. 48, 987–994. https://doi.org/10.2967/jnumed.107.039602.

Chung, H., Lee, J., Jeong, D., Han, I.-O., Oh, E.-S., 2012. Melanocortin 1 Receptor Regulates Melanoma Cell Migration by Controlling Syndecan-2 Expression. J. Biol. Chem. 287, 19326–19335. https://doi.org/10.1074/jbc.M111.334730.

Csupász, T., Lihi, N., Fekete, Z., Nagy, A., Botár, R., Forgács, V., Szikra, D., May, N.V., Tircsó, G., Kálmán, F.K., 2022. Exceptionally fast formation of stable rigidified cross-bridged complexes formed with Cu(II) isotopes for molecular imaging. Inorg. Chem. Front. 9, 1217–1223. https://doi.org/10.1039/D1QI01526E.

Dolg, M., Wedig, U., Stoll, H., Preuss, H., 1987. Energy-adjusted *a b i n i t i o* pseudopotentials for the first row transition elements. J. Chem. Phys. 86, 866–872. https://doi.org/10.1063/1.452288.

Dong, C., Feng, W., Xu, W., Yu, L., Xiang, H., Chen, Y., Zhou, J., 2020. The Coppery Age: Copper (Cu)-Involved Nanotheranostics. Adv. Sci. 7, 2001549. https://doi.org/10.1002/advs.202001549.

Ferdani, R., Stigers, D.J., Fiamengo, A.L., Wei, L., Li, B.T.Y., Golen, J.A., Rheingold, A.L., Weisman, G.R., Wong, E.H., Anderson, C.J., 2012. Synthesis, Cu(ii) complexation, ^{64} Cu-labeling and biological evaluation of cross-bridged cyclam chelators with phosphonate pendant arms. Dalton. Trans. 41, 1938–1950. https://doi.org/10.1039/C1DT11743B.

Frisch, M. J.; Trucks, G. W.; Schlegel, H. B.; Scuseria, G. E.; Robb, M. A.; Cheeseman, J. R.; Scalmani, G.; Barone, V.; Mennucci, B.; Petersson, G. A.; Nakatsuji, H.; Caricato, M.; Li, X.; Hratchian, H. P.; Izmaylov, A. F.; Bloino, J.; Zheng, G.; Sonnenberg, J. L.; Hada, M.; Ehara, M.; Toyota, K.; Fukuda, R.; Hasegawa, J.; Ishida, M.; Nakajima, T.; Honda, Y.; Kitao, O.; Nakai, H.; Vreven, T.; Montgomery Jr., J. A.; Peralta, J. E.; Ogliaro, F.; Bearpark, M. J.; Heyd, J.; Brothers, E. N.; Kudin, K. N.; Staroverov, V. N.; Kobayashi, R.; Normand, J.; Raghavachari, K.; Rendell, A. P.; Burant, J. C.; Iyengar, S. S.; Tomasi, J.; Cossi, M.; Rega, N.; Millam, N. J.; Klene, M.; Knox, J. E.; Cross, J. B.; Bakken, V.; Adamo, C.; Jaramillo, J.; Gomperts, R.; Stratmann, R. E.; Yazyev, O.; Austin, A. J.; Cammi, R.; Pomelli, C.; Ochterski, J. W.; Martin, R. L.; Morokuma, K.; Zakrzewski, V. G.; Voth, G. A.; Salvador, P.; Dannenberg, J. J.; Dapprich, S.; Daniels, A. D.; Farkas, Ö.; Foresman, J. B.; Ortiz, J. V.; Cioslowski, J.; Fox, D. J. Gaussian 09, Gaussian, Inc.: Wallingford, CT, USA, 2009., n.d.

Gao, F., Sihver, W., Jurischka, C., Bergmann, R., Haase-Kohn, C., Mosch, B., Steinbach, J., Carta, D., Bolzati, C., Calderan, A., Pietzsch, J., Pietzsch, H.-J., 2016. Radiopharmacological characterization of 64Cu-labeled α-MSH analogs for potential use in imaging of malignant melanoma. Amino. Acids 48, 833–847. https://doi.org/10.1007/s00726-015-2131-x.

Guo, H., Miao, Y., 2012. Cu-64-Labeled Lactam Bridge-Cyclized α-MSH Peptides for PET Imaging of Melanoma. Mol. Pharmaceutics 9, 2322–2330. https://doi.org/10.1021/mp300246j.

Hay, P.J., Wadt, W.R., 1985. *Ab initio* effective core potentials for molecular calculations. Potentials for K to Au including the outermost core orbitals. J. Chem. Phys. 82, 299–310. https://doi.org/10.1063/1.448975.

Heroux, K.J., Woodin, K.S., Tranchemontagne, D.J., Widger, P.C.B., Southwick, E., Wong, E.H., Weisman, G.R., Tomellini, S.A., Wadas, T.J., Anderson, C.J., Kassel, S., Golen, J.A., Rheingold, A.L., 2007. The long and short of it: the influence of N-carboxyethyl versusN-carboxymethyl pendant arms on in vitro and in vivo behavior of copper complexes of cross-bridged tetraamine macrocycles. Dalton. Trans. (21), 2150.

Hubin, T., 2003. Synthesis and coordination chemistry of topologically constrained azamacrocycles. Coord. Chem. Rev. 241, 27–46. https://doi.org/10.1016/S0010-8545(02)00307-7.

Hubin, T.J., McCormick, J.M., Collinson, S.R., Busch, D.H., Alcock, N.W., 1998. Ultra rigid cross-bridged tetraazamacrocycles as ligands—the challenge and the solution. ChemCommun. (16), 1675–1676.

Jadvar, H., Chen, X., Cai, W., Mahmood, U., 2018. Radiotheranostics in Cancer Diagnosis and Management. Radiology 286, 388–400. https://doi.org/10.1148/radiol.2017170346.

Kim, H.-J., Kim, D.-Y., Park, J.-H., Yang, S.-D., Hur, M.-G., Min, J.-J., Yu, K.-H., 2012. Synthesis and characterization of a 68Ga-labeled N-(2-diethylaminoethyl)benzamide derivative as potential PET Probe for malignant melanoma. Bioorg. Med. Chem. 20, 4915–4920. https://doi.org/10.1016/j.bmc.2012.06.047.

McIvor, J., Siew, T., Campbell, A., McCarthy, M., 2014. FDG PET in early stage cutaneous malignant melanoma: FDG PET in early stage melanoma. J. Med. Imaging. Radiat. Oncol. 58, 149–154. https://doi.org/10.1111/1754-9485.12173.

Miao, Y., Benwell, K., Quinn, T.P., 2007. 99mTc- and 111In-labeled alpha-melanocyte-stimulating hormone peptides as imaging probes for primary and pulmonary metastatic melanoma detection. J. Nucl. Med 48, 73–80.

Nagy, G., Dénes, N., Kis, A., Szabó, J.P., Berényi, E., Garai, I., Bai, P., Hajdu, I., Szikra, D., Trencsényi, G., 2017. Preclinical evaluation of melanocortin-1 receptor (MC1-R) specific 68Ga- and 44Sc-labeled DOTA-NAPamide in melanoma imaging. Eur. J. Pharm. Sci. 106, 336–344. https://doi.org/10.1016/j.ejps.2017.06.026.

Percie du Sert, N., Hurst, V., Ahluwalia, A., Alam, S., Avey, M.T., Baker, M., Browne, W. J., Clark, A., Cuthill, I.C., Dirnagl, U., Emerson, M., Garner, P., Holgate, S.T., Howells, D.W., Karp, N.A., Lazic, S.E., Lidster, K., MacCallum, C.J., Macleod, M., Pearl, E.J., Petersen, O.H., Rawle, F., Reynolds, P., Rooney, K., Sena, E.S., Silberberg, S.D., Steckler, T., Würbel, H., 2020. The ARRIVE guidelines 2.0: Updated guidelines for reporting animal research. PLoS Biol 18, e3000410. https://doi.org/10.1371/journal.pbio.3000410.

Pettersen, E.F., Goddard, T.D., Huang, C.C., Couch, G.S., Greenblatt, D.M., Meng, E.C., Ferrin, T.E., 2004. UCSF Chimera?A visualization system for exploratory research and analysis. J. Comput. Chem. 25, 1605–1612. https://doi.org/10.1002/jcc.20084.

Ren, G., Liu, Z., Miao, Z., Liu, H., Subbarayan, M., Chin, F.T., Zhang, L., Gambhir, S.S., Cheng, Z., 2009. PET of Malignant Melanoma Using ^{18} F-Labeled Metallopeptides. J. Nucl. Med 50, 1865–1872. https://doi.org/10.2967/jnumed.109.062877.

Rodriguez Rivera, A.M., Alabbas, H., Ramjaun, A., Meguerditchian, A.-N., 2014. Value of positron emission tomography scan in stage III cutaneous melanoma: A systematic review and meta-analysis. Surg. Oncol. 23, 11–16. https://doi.org/10.1016/j.suronc.2014.01.002.

Rodríguez-Guerra Pedregal, J., Gómez-Orellana, P., Maréchal, J.-D., 2018. ESIgen: Electronic Supporting Information Generator for Computational Chemistry Publications. J. Chem. Inf. Model. 58, 561–564. https://doi.org/10.1021/acs.jcim.7b00714.

Rosenkranz, A.A., Slastnikova, T.A., Durymanov, M.O., Sobolev, A.S., 2013. Malignant melanoma and melanocortin 1 receptor. Biochemistry. Moscow 78, 1228–1237. https://doi.org/10.1134/S0006297913110035.

Sandru, A., Voinea, S., Panaitescu, E., Blidaru, A., 2014. Survival rates of patients with metastatic malignant melanoma. J. Med. Life 7, 572–576.

Shircliff, A.D., Burke, B.P., Davilla, D.J., Burgess, G.E., Okorocha, F.A., Shrestha, A., Allbritton, E.M.A., Nguyen, P.T., Lamar, R.L., Jones, D.G., Gorbet, M.-J., Allen, M.B., Eze, J.I., Fernandez, A.T., Ramirez, D., Archibald, S.J., Prior, T.J., Krause, J.A., Oliver, A.G., Hubin, T.J., 2020. An ethylene cross-bridged pentaazamacrocycle and its Cu $^{2+}$ complex: constrained ligand topology and excellent kinetic stability. ChemCommun. 56, 7519–7522. https://doi.org/10.1039/D0CC00919A.

Tafreshi, N.K., Huang, X., Moberg, V.E., Barkey, N.M., Sondak, V.K., Tian, H., Morse, D. L., Vagner, J., 2012. Synthesis and Characterization of a Melanoma-Targeted Fluorescence Imaging Probe by Conjugation of a Melanocortin 1 Receptor (MC1R) Specific Ligand. Bioconjugate. Chem. 23, 2451–2459. https://doi.org/10.1021/bc300549s.

Thompson, S., Ballard, B., Jiang, Z., Revskaya, E., Sisay, N., Miller, W.H., Cutler, C.S., Dadachova, E., Francesconi, L.C., 2014. 166Ho and 90Y labeled 6D2 monoclonal antibody for targeted radiotherapy of melanoma: Comparison with 188Re

radiolabel. Nucl. Med. Biol. 41, 276–281. https://doi.org/10.1016/j.nucmedbio.2013.12.015.
Tomasi, J., Mennucci, B., Cammi, R., 2005. Quantum Mechanical Continuum Solvation Models. Chem. Rev. 105, 2999–3094. https://doi.org/10.1021/cr9904009.
Wallace, R.A., Dunn, T.J., Moore, D.A., 1995. Functionalized aza-macrobicyclic ligands for imaging applications. WO1995019185A1.
Weisman, G.R., Rogers, M.E., Wong, E.H., Jasinski, J.P., Paight, E.S., 1990. Cross-bridged cyclam. Protonation and lithium cation (Li+) complexation in a diamond-lattice cleft. J. Am. Chem. Soc. 112, 8604–8605. https://doi.org/10.1021/ja00179a067.
Weisman, G.R., Wong, E.H., Hill, D.C., Rogers, M.E., Reed, D.P., Calabrese, J.C., 1996. Synthesis and transition-metal complexes of new cross-bridged tetraamine ligands. ChemCommun. (8), 947.
Williams, H.A., Robinson, S., Julyan, P., Zweit, J., Hastings, D., 2005. A comparison of PET imaging characteristics of various copper radioisotopes. Eur. J. Nucl. Med. Mol. Imaging 32, 1473–1480. https://doi.org/10.1007/s00259-005-1906-9.
Woodin, K.S., Heroux, K.J., Boswell, C.A., Wong, E.H., Weisman, G.R., Niu, W., Tomellini, S.A., Anderson, C.J., Zakharov, L.N., Rheingold, A.L., 2005. Kinetic Inertness and Electrochemical Behavior of Copper(II) Tetraazamacrocyclic Complexes: Possible Implications for in Vivo Stability. Eur. J. Inorg. Chem. 2005, 4829–4833. https://doi.org/10.1002/ejic.200500579.
Zhang, C., Lin, K.-S., Bénard, F., 2017a. Molecular Imaging and Radionuclide Therapy of Melanoma Targeting the Melanocortin 1 Receptor. Mol Imaging 16, 153601211773791. https://doi.org/10.1177/1536012117737919.
Zhang, C., Zhang, Z., Lin, K.-S., Pan, J., Dude, I., Hundal-Jabal, N., Colpo, N., Bénard, F., 2017b. Preclinical Melanoma Imaging with ^{68} Ga-Labeled α-Melanocyte-Stimulating Hormone Derivatives Using PET. Theranostics 7, 805–813. https://doi.org/10.7150/thno.17117.
Zhou, J.Y., Prognon, P., 2006. Raw material enzymatic activity determination: A specific case for validation and comparison of analytical methods—The example of superoxide dismutase (SOD). J. Pharm. Biomed. Anal. 40, 1143–1148. https://doi.org/10.1016/j.jpba.2005.09.022.